

Compensation of temperature effect on impedance responses of PZT interface for prestress-loss monitoring in PSC girders

Thanh-Canh Huynh and Jeong-Tae Kim*

*Department of Ocean Engineering, Pukyong National University, 599-1 Daeyeon 3-dong,
Nam-gu, Busan 608-737, Republic of Korea*

(Received November 21, 2015, Revised April 6, 2016, Accepted April 11, 2016)

Abstract. In this study, a method to compensate the effect of temperature variation on impedance responses which are used for prestress-loss monitoring in prestressed concrete (PSC) girders is presented. Firstly, an impedance-based technique using a mountable lead-zirconate-titanate (PZT) interface is presented for prestress-loss monitoring in the local tendon-anchorage member. Secondly, a cross-correlation-based algorithm to compensate the effect of temperature variation in the impedance signatures is outlined. Thirdly, lab-scale experiments are performed on a PSC girder instrumented with a mountable PZT interface at the tendon-anchorage. A series of temperature variation and prestress-loss events are simulated for the lab-scale PSC girder. Finally, the feasibility of the proposed method is experimentally verified for prestress-loss monitoring in the PSC girder under temperature-varying conditions and prestress-loss events.

Keywords: impedance monitoring; mountable PZT interface; prestress force monitoring; tendon-anchorage; PSC girders; temperature effect; temperature compensation

1. Introduction

Over the past decades, damage monitoring in structural systems by using local impedance properties has been studied by many researchers (Liang *et al.* 1994, Sun *et al.* 1995, Zagari and Giurgiutiu 2001, Fasel *et al.* 2005, Kim *et al.* 2006, Nguyen and Kim 2012, Li *et al.* 2014). The impedance-based method utilizes the electro-mechanical (EM) impedance of a coupled piezoceramic patch - structure system as the local dynamic feature to detect incipient damage at local critical regions. Recently, the impedance-based method has been applied for monitoring prestress-loss in prestressed structures by detecting the change in impedance responses at the anchorage zone (Kim *et al.* 2006, Kim *et al.* 2010, Nguyen *et al.* 2012, Min *et al.* 2012, and Huynh *et al.* 2015a). An issue of the impedance-based technique is on setting the effective frequency band which is sensitive to the change of structural parameters. The impedance monitoring conducted on a prestressed concrete (PSC) girder showed that the effective frequency band was even over 800 kHz for a mono-tendon anchorage under compressive forcing about 100 kN (Kim *et al.* 2010).

As an alternative monitoring technique for the tendon-anchorage, Nguyen and Kim (2012) proposed a lead-zirconate-titanate (PZT) interface device which could reduce the sensitive

*Corresponding author, Professor, E-mail: idis@pknu.ac.kr

frequency band of impedance responses to below 100 kHz and also the need of high performance impedance analyzers. However, the design of PZT interface should be installed during the construction of the anchorage system, so it is impossible to apply it into existing joint members. To overcome the limitation, Huynh and Kim (2014) proposed a mountable PZT interface that can be installed on and detached from existing tendon-anchorage systems. The proposed interface device was numerically and experimentally evaluated for a lab-scaled prestressed structure to monitor the change in impedance responses caused by the change in prestress forces (Huynh and Kim 2014, Huynh *et al.* 2015b). The mountable PZT interface can be integrated with the wireless sensor technology to achieve an automated, cost-efficient monitoring system for real applications (Lynch *et al.* 2006, Mascarenas 2007, Rice *et al.* 2010, Ho *et al.* 2012, Kim *et al.* 2014, Huynh *et al.* 2016). However, this fact also leads to an important issue that needs to be solved before real field applications. That is the performance of the mountable PZT interface under the temperature variation since boundary conditions and material constants of both PZT interface devices and host structures are temperature-dependent.

Many researchers have worked on examining the effect of temperature variation on structural dynamic properties that are utilized for structural health monitoring (Park *et al.* 1999, Kim *et al.* 2003, Ko and Ni 2005, Sohn 2007, Kim *et al.* 2013, Fabricio *et al.* 2014, Huynh *et al.* 2015c, Huynh and Kim 2016). Temperature-induced variability of local impedance responses should also be quantified in the determination of impedance features that are used for damage monitoring (Park *et al.* 1999, Koo *et al.* 2009, and Hong *et al.* 2011, Yun *et al.* 2013, Park *et al.* 2015). Park *et al.* (1999) presented that any changes in environmental temperature can lead to horizontal and vertical shifts of resonant impedance signatures. To remove the temperature effect from damage detection results, Park *et al.* (1999) used a modified root-mean-square-deviation (RMSD) index based on the concept of effective frequency shift (EFS).

By employing the EFS concept, Koo *et al.* (2009) proposed a maximum cross-correlation (CC) index to minimize the variation in impedance signatures caused by the variation of temperatures. An issue of the EFS-based technique is on selecting the frequency range which should be sensitive to damage but sufficiently narrow for the temperature compensation (Fabricio *et al.* 2014). Sepehry *et al.* (2011) and Yun *et al.* (2013) used artificial neural networks (ANNs) to compensate the temperature effect for impedance-based fault detection. However, the ANNs needs to be trained with multiple sets of measurements under varying temperatures for not only healthy but also damaged scenarios. For existing structures, moreover, it is almost impossible to acquire suitable training patterns of the ANNs for the damaged states unless target structures can be accurately modeled for finite element analyses.

This study has been motivated to monitor the loss of prestress forces in PSC girders by using impedance responses measured under temperature-varying conditions. Firstly, an impedance-based technique using a mountable PZT interface is presented for prestress-loss monitoring in the local tendon-anchorage member. Secondly, a cross-correlation-based algorithm to compensate the effect of temperature variation in the impedance signatures is outlined. Thirdly, lab-scale experiments are performed on a PSC girder instrumented with a mountable PZT interface at the tendon-anchorage. A series of temperature variation and prestress-loss events are simulated for the lab-scale PSC girder. Finally, the feasibility of the proposed method is experimentally verified for prestress-loss monitoring in the PSC girder under temperature-varying conditions and prestress-loss events.

2. Prestress-loss monitoring by impedance responses of mountable PZT interface

The mountable PZT interface was proposed to alternatively monitor EM impedance signatures of the prestressed tendon-anchorage system (Huynh and Kim 2014). As illustrated in Fig.1, the interface device is mounted on the bearing plate’s surface which is compressed by the anchoring force. This interface has the fixed-fixed boundary condition by two outside contact bodies and the flexible beam section in the middle, as shown in Fig. 1 (Huynh *et al.* 2015c). The structural properties of the PZT interface are basically selected to fulfil the limitation of the issue on selecting effective frequency band for the impedance-based method. In this study, the PZT interface is designed to deal with 1V-amplitude excitation and impedance monitoring using wireless sensor technology allows the frequency range of 10-100 kHz (Mascarenas *et al.* 2007, Park *et al.* 2010).

Fig. 2 illustrates the interaction between the PZT patch and the structure (e.g., the interface body) from which the structural mechanical (SM) impedance response can be explained (Huynh *et al.* 2015c). An input harmonic voltage $V(\omega)$ induces a deformation of the PZT due to the inverse piezoelectric effect. Then a force $F(\omega)$ against that deformation is induced into the structure (i.e., the interface body) and the PZT as well, because the PZT is surface-bonded to the interface structure. The SM impedance of the structure is defined as the ratio of force $F(\omega)$ to velocity $\dot{u}(\omega)$ as follows (Liang *et al.* 1994)

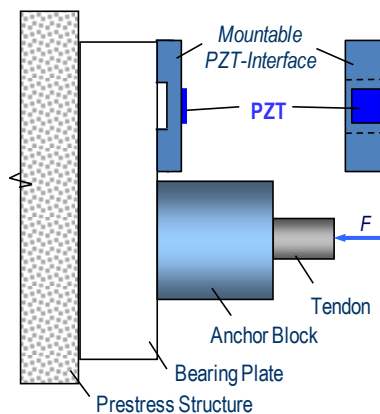


Fig. 1 Prestressed tendon-anchorage system with a mountable PZT interface

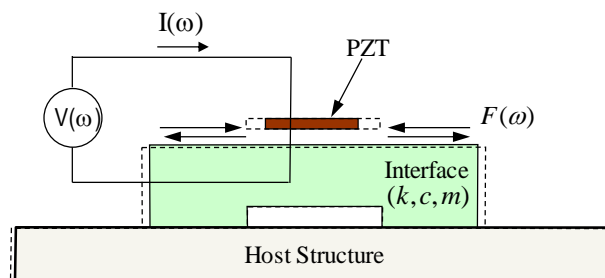


Fig. 2 PZT interface-structure model for SM impedance response

$$Z_s(\omega) = \frac{F(\omega)}{\dot{u}(\omega)} = c + m \frac{\omega^2 - \omega_n^2}{\omega} i \quad (1)$$

where c and m are the damping coefficient and the mass of the interfacing structure with the PZT patch, respectively; ω_n is the angular natural frequency of the interface structure; and ω is the angular frequency of the excitation voltage. The SM impedance is a function of structural properties (i.e., mass, damping, and stiffness), so that the change in structural parameters can be inversely interpreted by the change in the SM impedance.

In practice, the electric current $I(\omega)$ is measured and then it is utilized to calculate electro-mechanical (EM) impedance, as described below (Liang *et al.* 1994)

$$Z(\omega) = \frac{V}{I} = \left\{ i\omega \frac{w_a l_a}{t_a} \left[\hat{\varepsilon}_{33}^T - \frac{1}{Z_a(\omega)/Z_s(\omega) + 1} d_{3x}^2 \hat{Y}_{xx}^E \right] \right\}^{-1} \quad (2)$$

where $\hat{Y}_{xx}^E = (1 + i\eta)Y_{xx}^E$ is the complex Young's modulus of the PZT patch at zero electric field; $\hat{\varepsilon}_{xx}^T = (1 - i\delta)\varepsilon_{xx}^T$ is the complex dielectric constant at zero stress; d_{3x} is the piezoelectric coupling constant in x-direction at zero stress; and w_a , l_a , and t_a are the width, length, and thickness of the PZT patch, respectively. The parameters η and δ are structural damping loss factor and dielectric loss factor of piezoelectric material, respectively. Eq. (2) shows that the EM impedance, $Z(\omega)$, is a combining function of the SM impedance of the piezoelectric patch, $Z_a(\omega)$, and that of the host structure (e.g., the interface), $Z_s(\omega)$. The SM impedance is a function of mass, damping, and stiffness (i.e., stiffness is introduced from natural frequency, $k = m\omega_n^2$), as shown in Eq. (1). Thus, the change in structural parameters (m , k and c) caused by environmental conditions and damage can be represented by the change in the EM impedance. As proved in the related publication (Nguyen and Kim 2012), the contribution of the SM impedance to the EM impedance is considerable when the excitation frequency is identical to the natural frequency of the structure (i.e., $\omega = \omega_n$). At the resonant frequency, the SM impedance takes the damping coefficient as the contribution to the EM impedance ($Z_s(\omega) = c$). To sensitively identify the change in structural properties, therefore, the EM impedance should be monitored in the resonant frequency range.

For the 'PZT interface-bearing plate-anchor force' system as illustrated in Fig. 1, the change of the anchorage force may cause the change of the bearing plate's structural properties such as geometrical and tractional boundary conditions. This structural change of the bearing plate could lead to the change of the PZT interface's properties such as geometrical and stress boundary conditions. Consequently, local dynamic characteristics of the PZT interface could be changed due to the variation of tendon force. In other words, the anchoring force could be monitored by the local impedance responses of the PZT interface device mounted on the surface boundary of the bearing plate.

3. EFS-Based temperature-effect compensation technique

Previous experimental studies reported that the temperature change causes not only the frequency shift but also the amplitude shift of resonant impedance signatures since boundary conditions and material constants of both interface devices and host structures are temperature-dependent (Park *et al.* 1999, Koo *et al.* 2009, Fabricio *et al.* 2014). Consequently, the

damage indices (i.e., RMSD, CCD) can be much higher than 0 even for a healthy structure, leading to a false positive diagnosis.

Koo *et al.* (2009) utilized the concept of EFS (Park *et al.* 1999) to develop a temperature-effect compensation method for minimizing false positive diagnoses. The EFS-based technique (Koo *et al.* 2009) has continued to be adopted in recent damage detection works (Yun *et al.* 2013, Siebel and Lilov 2013, Fabricio *et al.* 2014) since it requires simple computations and can be utilized for general impedance-based applications. The EFS-based technique compensates the temperature effect by shifting an effective frequency ($\delta\omega$) to give the minimum correlation coefficient deviation (CCD) between the baseline impedance signature, $Z_o(\omega)$, and the current impedance signature after temperature change, $Z_1(\omega)$. The CCD index after the EFS (CCD_{EFS}) is calculated as follows

$$CCD_{EFS} = \min_{\delta\omega} \left\{ 1 - \frac{E \left\{ \left[\text{Re}(Z_o(\omega_i)) - \text{Re}(\bar{Z}_o) \right] \left[\text{Re}(Z_1(\omega_i - \delta\omega)) - \text{Re}(\bar{Z}_1) \right] \right\}}{\sigma_{Z_o} \sigma_{Z_1}} \right\} \quad (3)$$

in which $E[\cdot]$ is the expectation operation; $\text{Re}(Z_o(\omega_i))$ and $\text{Re}(Z_1(\omega_i))$ signifies the real parts of the EM impedances of the i^{th} frequency; $\text{Re}(\bar{Z}_o)$ and $\text{Re}(\bar{Z}_1)$ signify the mean values of impedance signatures (real part); and σ_{Z_o} and σ_{Z_1} are the standard deviation values. A loop routine is performed until the value of the minimum CCD is obtained.

Fig. 3 shows an ideal scenario for impedance monitoring with the EFS-based temperature compensation. For the intact state under temperature variation, the temperature change (δT) causes approximately the same frequency shift ($\delta\omega_{\delta T}$) of the resonant impedance peaks (see Fig. 3(a)). Meanwhile, the damage state under temperature change induces the different frequency shift ($\delta\omega_{d+\delta T}$) of the resonant peaks (see Fig. 3(b)). After the EFS compensation, consequently, the CCD_{EFS} index of the damage state could be much more significant than that of the intact state under the temperature variation. By this way, the structural damage under varying temperature conditions could be alarmed.

Ideally, the CCD index after the EFS (i.e., CCD_{EFS}) is almost equal to 0 for the undamaged scenario under temperature variation, and larger than 0 if damage occurs. However, due to experimental and computational errors, the damage index CCD_{EFS} could be larger than 0 although damage is not occurred. For dealing with these uncertain conditions, a control chart analysis is employed for decision-making out of the CCD_{EFS} index's values. An upper control limit (UCL) of the damage index CCD_{EFS} is adopted for alarming the damage occurrence, as follows

$$UCL = \mu + 3\sigma \quad (4)$$

where μ and σ are mean and standard deviation of the damage index CCD_{EFS} at undamaged condition, respectively. In Eq. (4), the UCL is determined by three standard deviations of the mean, which is corresponding to 99.7% confidence level (Hong *et al.* 2011, Huynh and Kim 2014). The occurrence of damage is indicated when the damage index after the temperature compensation (CCD_{EFS}) is larger than the control limit (UCL). Otherwise, there is no indication of damage occurrence.

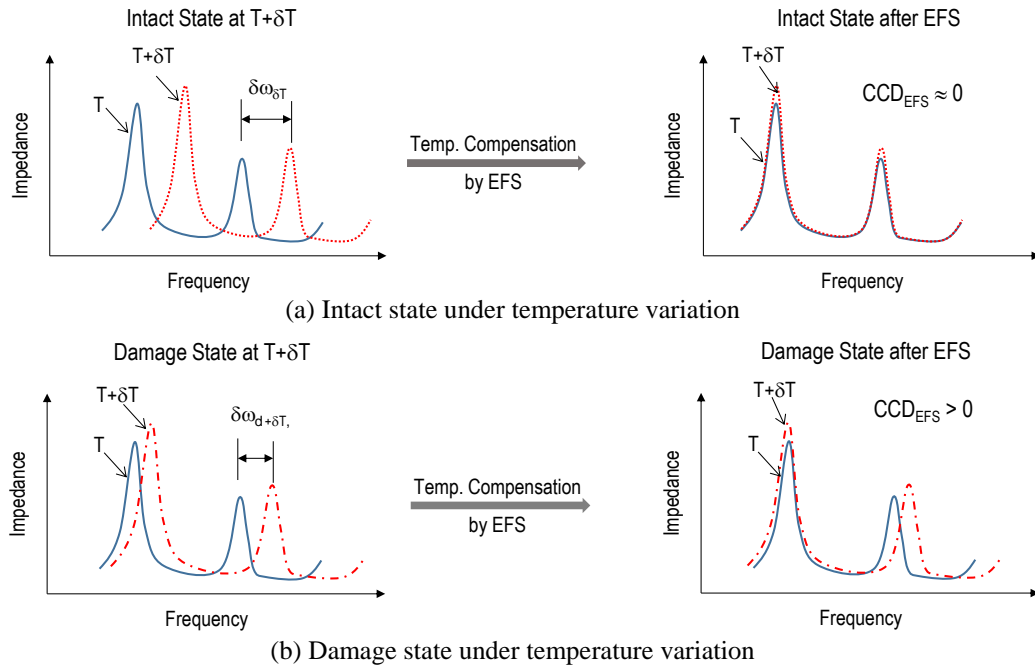


Fig. 3 An ideal scenario for impedance monitoring with EFS-based temperature compensation

4. Experiments on PSC girder

4.1 Test-setup of PSC girder

Lab-scale experiments were conducted on a 6.4-meter PSC girder instrumented with a mountable PZT interface at the tendon-anchorage, as shown in Fig. 4(a). The tested T-section girder was simply supported by the steel bars at both ends. The 28-day compressive strength of the concrete was 23.6 MPa, and the mass density was approximately 2400 kg/m³. The PSC girder was eccentrically prestressed by a 7-wire straight tendon. The prestress forces were introduced into the tendon by a stressing jack as the tendon was anchored at one end and pulled out at the other. A load cell was installed at the left end to measure the applied prestress force. As shown in Fig. 4(b), an aluminum PZT Interface was designed and surface-bonded to the bearing plate of the right anchorage. For temperature measurement, a K-type thermocouple wire was setup on the top surface of the PSC girder, see Fig. 4(c).

The tendon was first pre-tensioned to 138.3 kN (14.1 ton) for the intact state. For each test, the PZT patch on the interface was excited by a harmonic excitation voltage with 1V-amplitude, and the impedance signature was measured by an impedance analyzer HIOKI 3532, as illustrated in Fig. 5(a). The impedance analyzer was set for automatically measuring every 10 minutes with the swept frequency within 10 ~ 55 kHz. A static data logger (Kyowa EDX-100A) was used to monitor temperature via the K-type thermocouple wire, as shown in Fig. 5(b). The 1 Hz sampling rate was set for the temperature measurement system during the tests.

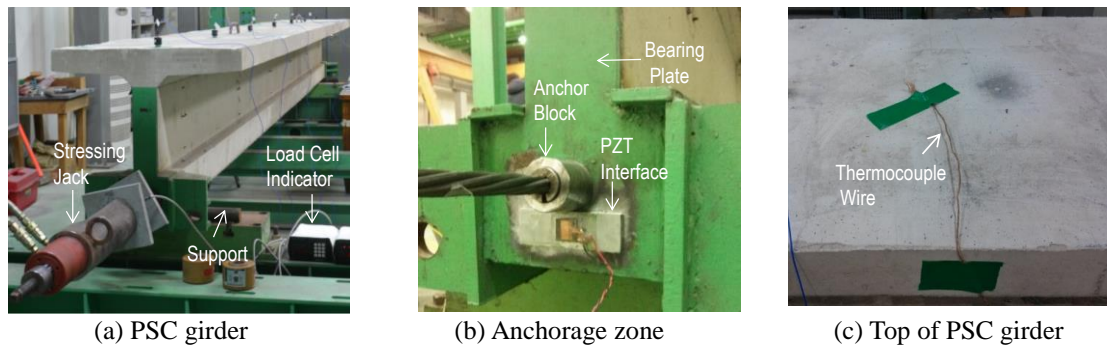


Fig. 4 Experimental setup in PSC girder

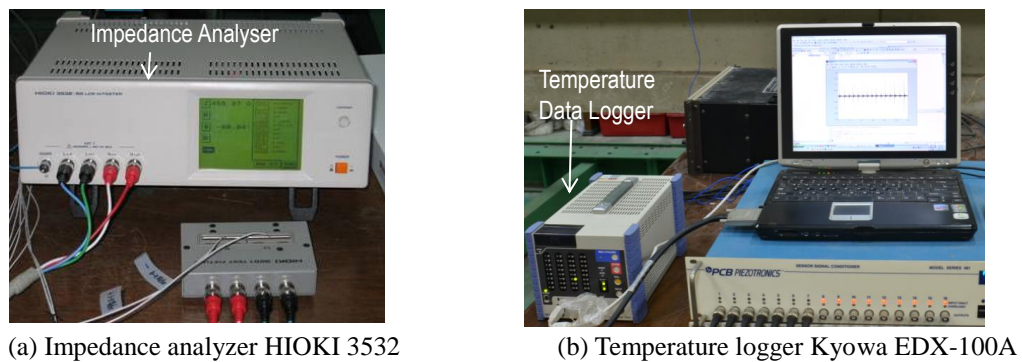


Fig. 5 Impedance and temperature measurement systems

4.2 Simulations of temperature variation and prestress-Loss

In order to analyze the variation in impedance responses under fluctuating temperature conditions, and to compensate the temperature effect in the impedance-based prestress-loss monitoring results, firstly, temperature variation with a fixed prestress force is simulated for the PSC girder in the underground laboratory; secondly, various prestress-loss events are conducted in the PSC girder at a specific temperature of the laboratory.

4.2.1 Simulation of temperature variation

As the first test scenario, the laboratory temperature was controlled to vary between 6.72°C to 22.33°C while the tendon force was set fixed as 138.3 kN. A series of tests were performed for seven consecutive days from 28 January to the midday of 04 February, 2015 including two days for heating and five days for continuously auto-monitoring. The time history of the temperature variation simulated in the laboratory is shown in Fig. 6. At the beginning, the heaters were turn on to heat the temperature of the underground laboratory up as designed. The impedance tests started at 21:00 hour of January 29, 2015 as the laboratory temperature reached up to 22.33°C. Then the room temperature was controlled to decrease gradually by turning off the heaters for the five

remaining 5 days. It is noted that the room temperature changed day and night, as shown in Fig. 6. Totally, 669 measurement tests were performed on the PZT interface.

4.2.2 Simulation of prestress-loss

The impedance and temperature measurements were monitored continuously after the first test scenario. As the second test scenario, the room temperature was then controlled almost constant by air conditioners in the laboratory. Fig. 7 shows the time history of the measured temperature during the second test period on 04 January, 2015. As observed from the figure, the temperature variation was very small, about 1°C during the experimental tests. While the laboratory temperature was handled to almost constant of 19.5°C , a set of prestress-loss scenarios was simulated to the PSC girder from which the impedance responses of the PZT interface were measured for detecting the prestress-loss. Five prestressing levels: PS1 = 138.3 kN, PS2 = 128.5 kN, PS3 = 117.7 kN, PS4 = 108.9 kN, and PS5 = 99.1 kN were set for the test structure. By each prestressing level, five sets of impedance data were sampled. Totally, 25 sets of impedance data were acquired from the PZT interface.

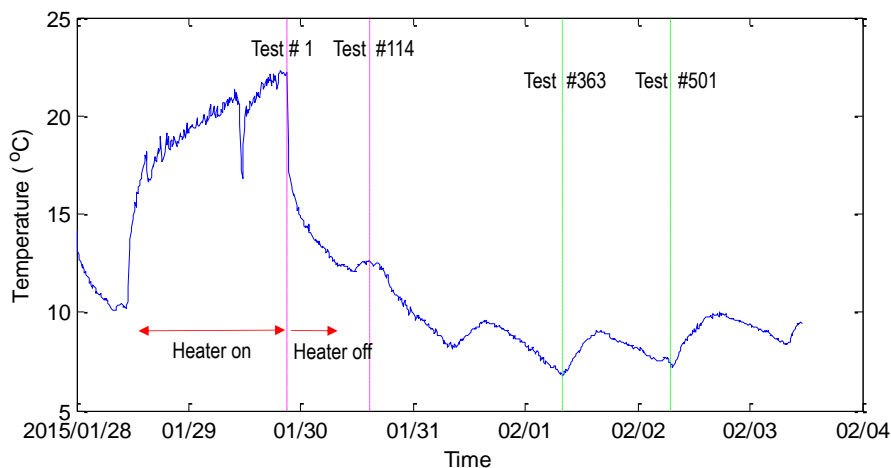


Fig. 6 Temperature variation simulated in laboratory

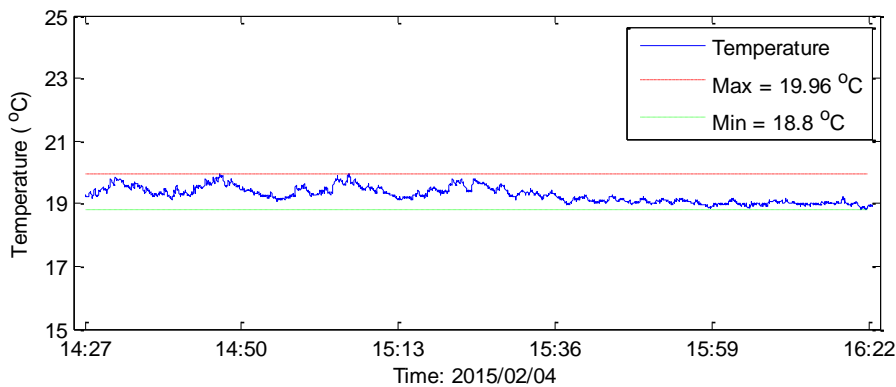


Fig. 7 Near-constant temperatures during prestress-loss simulation

5. Prestress-loss monitoring under constant temperature

5.1 Impedance responses of mountable PZT interface under prestress-loss scenarios

To evaluate the feasibility of the mountable PZT interface-based prestress-loss monitoring in PSC girders, the impedance signatures measured during the prestress-loss simulation under constant temperature (i.e., the second test scenario) are used for computing damage indices. Figure 8(a) shows real impedance signatures of the PZT interface in the frequency range of 10 kHz - 55 kHz (901 interval points) for the healthy state PS1 and four damage cases PS2 ~ PS5 under the constant temperature. Two resonant frequency ranges of 10-22 kHz, and 25-35 Hz are plotted in Figs. 8(b) and 8(c), respectively. As observed from these figures, the resonant peaks tended to sensitively shift left according to the decrement of prestress force. This indicates that modal stiffness of the PZT interface decreased with the prestress-loss of the PSC girder.

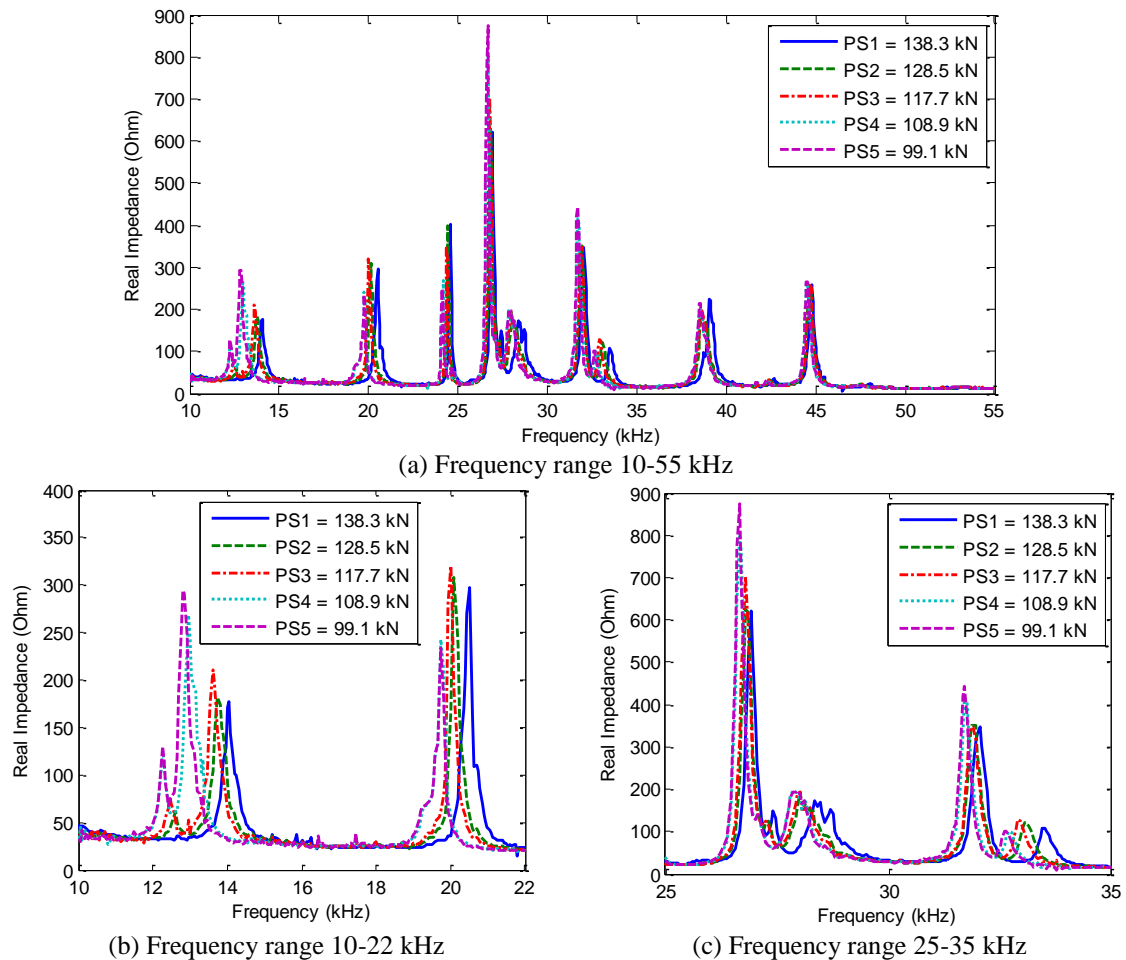


Fig. 8 Impedance signatures of PZT interface under various prestress forces

As compared to the impedance signatures of the same mountable PZT interface in the previous study (Huynh and Kim 2014), the current impedance signatures have more resonant peaks. This implies that the contribution of the SM impedance to the EM impedance was considerable over this frequency range, as explained in Eq. (2). The comparison between the modal analysis and the impedance analysis of the mountable PZT interface (Huynh *et al.* 2015b) showed that some vibration modes were absent from the impedance signatures. The reason is that the damping coefficients of these modes were much more significant than the mechanical impedance of the PZT sensor. This led to negligible contributions of the SM impedance to the EM impedance, as explained by Eq. (2). In this study, the target structure and the bonding layer of the PZT interface differed from the previous ones, resulting different damping coefficients of some vibration modes. Therefore, some resonant peaks in the previous impedance may not be absent in the current impedance.

5.2 Prestress-loss monitoring results under constant temperature

In impedance-based method, wide frequency bands containing many resonant peaks should be selected for the impedance-based damage detection (Park *et al.* 1999). Fig. 9 shows the RMSD and CCD indices of the impedance signatures in the frequency range 10-55 kHz computed for five prestressing levels (PS1 ~ PS5). Details on computing the RMSD and CCD indices can be found in existing publications (Sun *et al.* 1995, Zagrai and Giurgiutiu 2001). It is worthy to note that the RMSD and CCD indices were the mean values obtained from five repeated measurements of each test. It is clear that both RMSD and CCD indices increased sensitively with the reduction of tendon force.

As observed from Fig. 9, the RMSD and CCD indices successfully alarmed the loss of prestress forces in the PSC girder when the damage indices of damage cases were significantly higher than the UCL level. It is also found that the RMSD index were higher than the CCD index over the considered frequency band. Therefore, the RMSD index could be a better damage indicator for the impedance monitoring under constant temperature. This experimental evaluation has proved the feasibility of the mountable PZT interface for prestress-loss monitoring in PSC girders under unchanged environmental conditions.

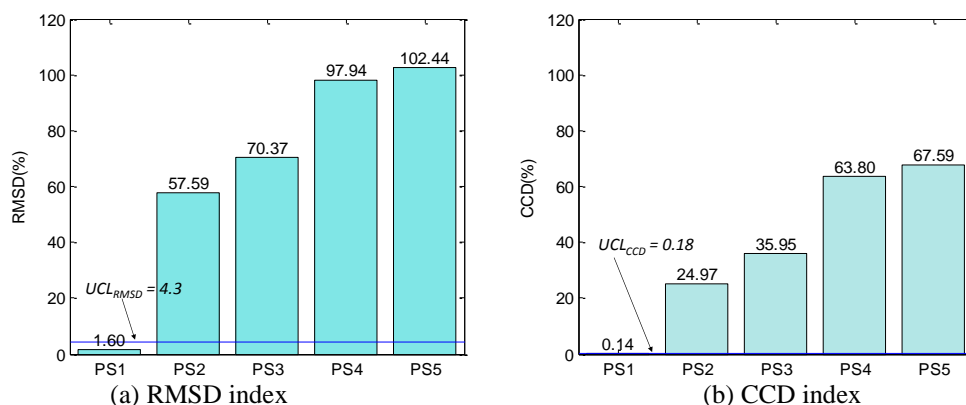


Fig. 9 Prestress force-loss monitoring results under constant temperatures

6. Prestress-loss monitoring under temperature variation

6.1 Temperature effect on impedance signatures of mountable PZT interface

As described earlier, the impedance signatures and the temperature data were monitored continuously during the two test scenarios. For the temperature-effect compensation, the total number of impedance measurements is 694 including 669 for the intact state (i.e., the first test scenario) and 25 for the five prestress levels (i.e., the second test scenario). Fig. 10 shows the 669 impedance measurements for the baseline (intact) state. The real impedance signatures were carried out for the frequency range 10-55 kHz under the temperature variation $6.72^{\circ}\text{C} \sim 22.33^{\circ}\text{C}$. It is found that the temperature variation caused significant horizontal shifts of the impedance signals. Within the frequency range of 10-55 kHz, several resonant peaks of the impedance signatures were taken into account. As plotted in Fig. 11, the amplitude of the impedance signatures varied significantly as the temperature changed.

Temperature effects come in various sources, including materials, boundary conditions, mountable interface and PZT sensor itself. The temperature change causes the change in the stress field of the anchorage zone, the mountable interface and the PZT sensor. Its temperature change also causes the variation in the electrical impedance of the PZT sensor. As the result, the local impedance response is varied with the temperature. Moreover, each resonant frequency has the different nature under the temperature change, due to its sensitivity to the changes in the structural parameters (i.e., materials and boundary conditions) caused by the temperature variation (Kim *et al.* 2003). As the result, some resonant frequency bands of the impedance response may show less variations with the temperature changes than others (Fabricio *et al.* 2014), as shown in Figs. 10 and 11.

The impedance signatures in 25-30 kHz of the intact and prestress-loss states at different temperatures were plotted in Fig. 12. As shown in the figure, the resonant peaks shifted right as the temperature increased from 12.63°C to 19.49°C for intact states, but they shifted left for the prestress-loss states. The reason comes from the difference in the thermal expansion coefficients of the aluminum interface ($\alpha_{\text{Al}} = 22.2 \times 10^{-6} \text{ m/m}^{\circ}\text{C}$) and the steel bearing plate ($\alpha_{\text{Fe}} = 12 \times 10^{-6} \text{ m/m}^{\circ}\text{C}$) at the anchorage zone. Under the same temperature change, the aluminum interface expands more than the steel bearing plate. Since the interface was fixed on the bearing plate, the different expansion capacities of the materials led to an additional stress field in the interface.

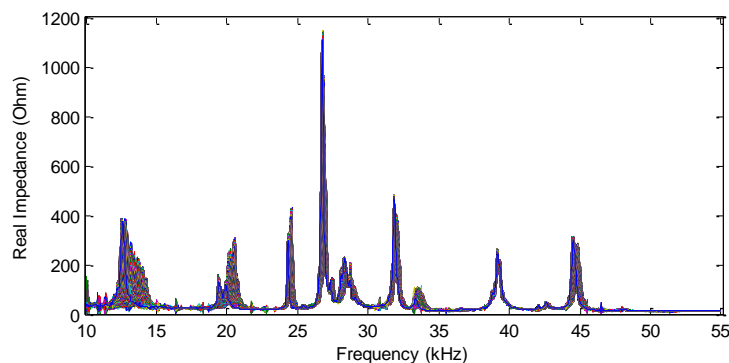


Fig. 10 Impedance signatures for frequency range 10-55 kHz measured from intact tendon-anchorage for temperatures: $6.72^{\circ}\text{C} \sim 22.33^{\circ}\text{C}$

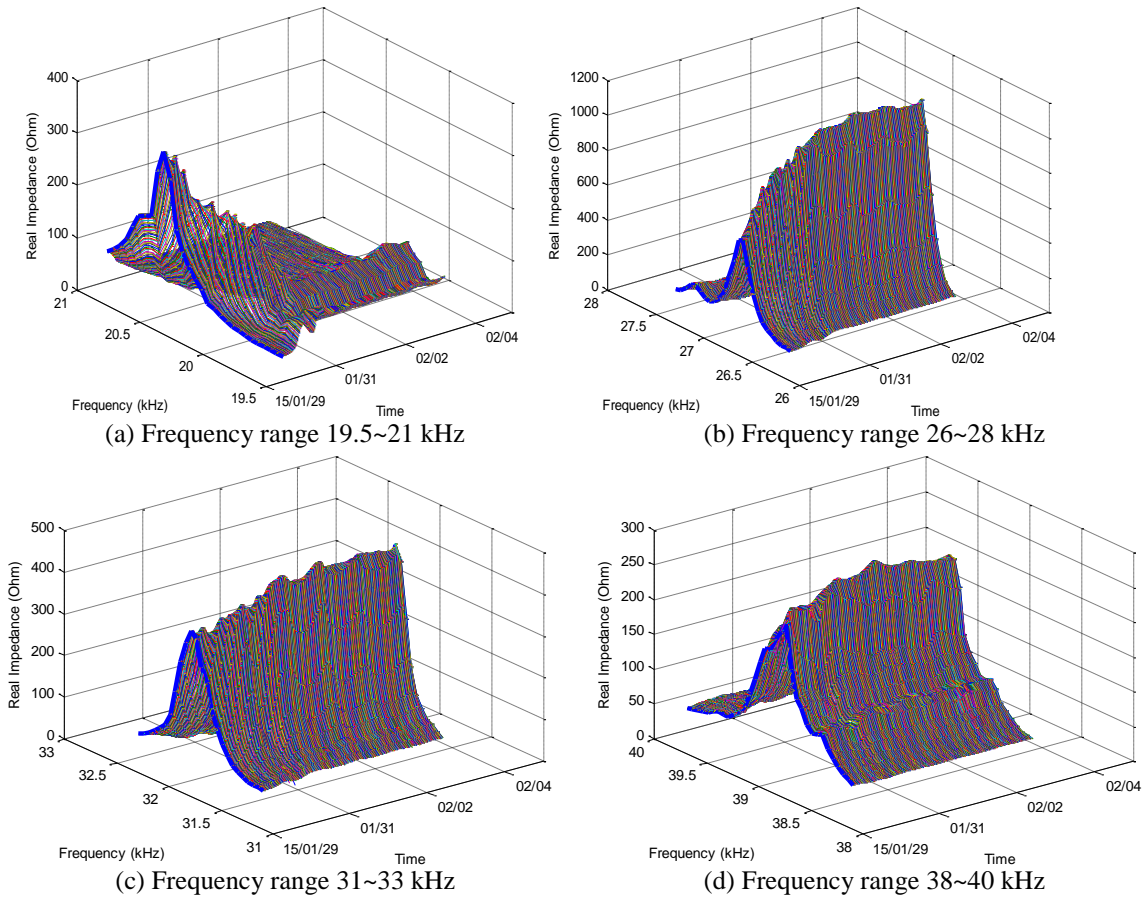


Fig. 11 Time history of resonant peaks of impedance signatures measured from intact tendon-anchorage for temperatures: 6.72°C ~ 22.33°C

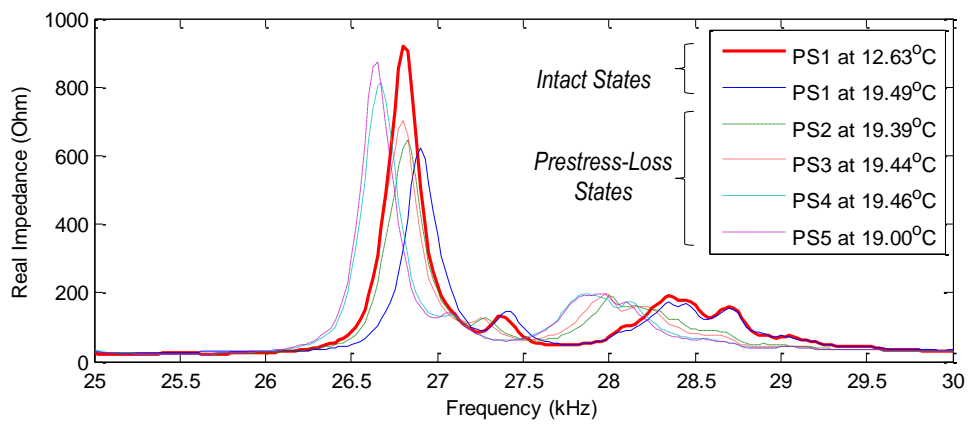


Fig. 12 Impedance signatures in 25-30 kHz for intact and prestress-loss states under varying temperatures

As the result, the resonant peaks of the interface shifted right when the temperature increased. As explained previously, the resonant peaks shifted left for the prestress-loss states due to the decrement in the modal stiffness of the interface. It is unknown at this time whether the change in the impedance signatures of the scenarios PS2~PS5 was induced by the prestress-loss events or the varying temperature conditions. Unless the temperature effect is compensated, therefore, the impedance monitoring could lead to false diagnostic results for the prestress-loss occurrence.

6.2 Frequency ranges for temperature compensation

An important issue of the EFS-based technique is on pre-determining the resonant frequency range which should be sensitive to structural changes for the damage detection and sufficiently narrow for the temperature compensation. A good match between the compensated impedance signatures and the baseline impedance signatures can be observed if the resonant peaks in the monitored frequency band exhibit approximately the same frequency shift. To minimize the false-alarm of the impedance monitoring due to the uncertain temperature conditions, a selecting process is performed to select an appropriate frequency range among various frequency bands for the temperature compensation. Firstly, potential frequency ranges which contain resonant impedance peaks are selected. Secondly, CCD indices of these potential frequency ranges are computed under varying temperatures. Finally, according to the relationships between the CCD index and the temperature, the frequency range that shows less variation with the temperature change is selected for the temperature-effect compensation.

Fig. 13 shows comparisons between the impedance signatures of Test 1 and Test 114 in 12-47 kHz, which were respectively measured from the intact tendon-anchorage at 22.33°C and 12.63°C (about 10°C variation). More details on the number of the impedance measurement can be found in Fig. 6. Before the temperature compensation, a considerable CCD value of 37.8% can be observed between two impedance signatures. To remove the temperature effect, the impedance signatures of Test 114 was shifted to fit with those of Test 1 (i.e., reference impedance pattern) using the EFS-based technique. After the EFS, however, the CCD value still remained significant as 16.7%. It's worth noting that the real part of the impedance responses was used to calculate the CCD index and the impedance patterns after the EFS were normalized to unity for the comparison.

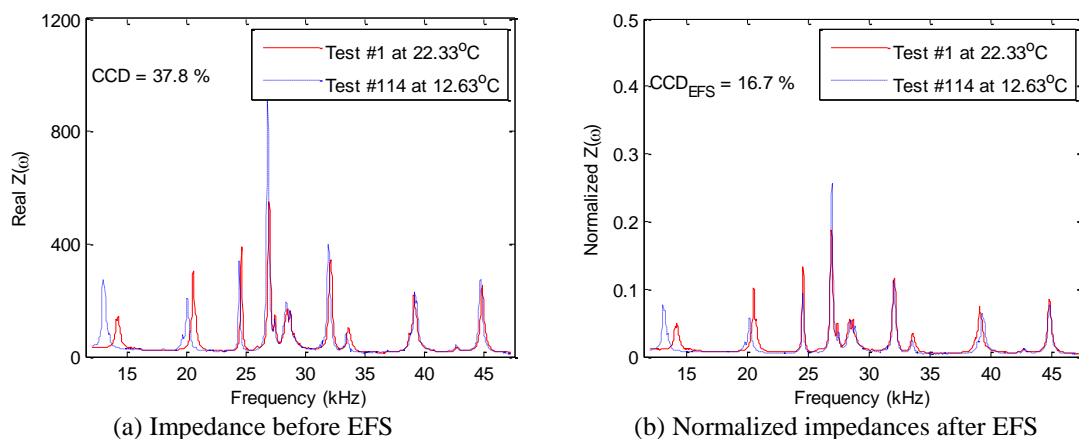


Fig. 13 Impedance signatures for frequency range 12-47 kHz measured from intact tendon-anchorage for two different temperatures: 22.33°C versus 12.63°C (Reference: Test #1)

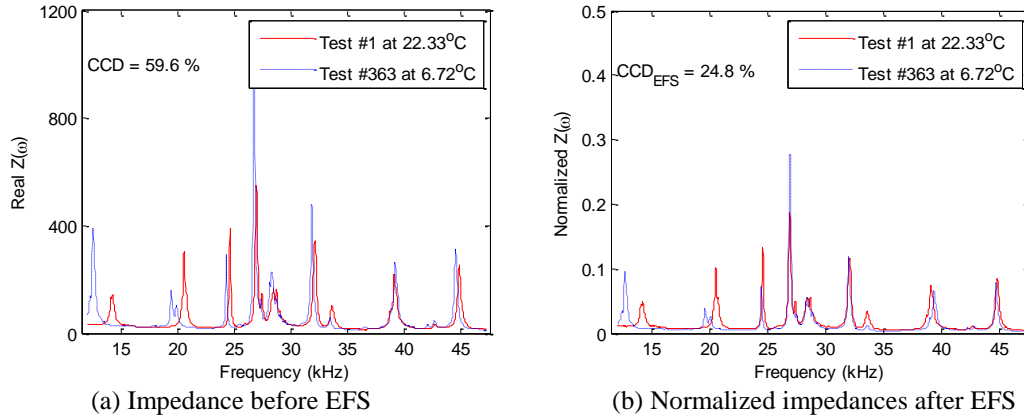


Fig. 14 Impedance signatures for frequency range 12-47 kHz measured from intact tendon-anchorage for two temperatures: 22.33°C versus 6.72°C (Reference: Test #1)

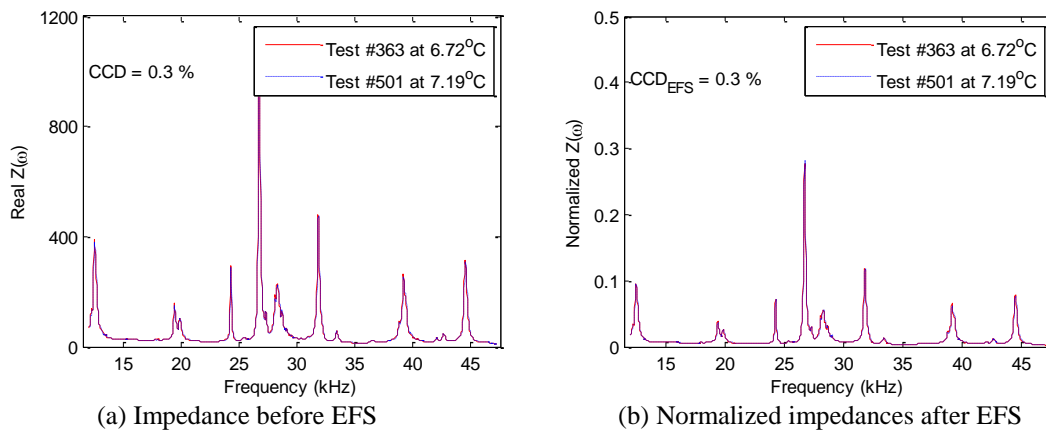


Fig. 15 Impedance signatures for frequency range 12-47 kHz measured from intact tendon-anchorage for two close temperatures: 6.72°C versus 7.16°C (Reference: Test #363)

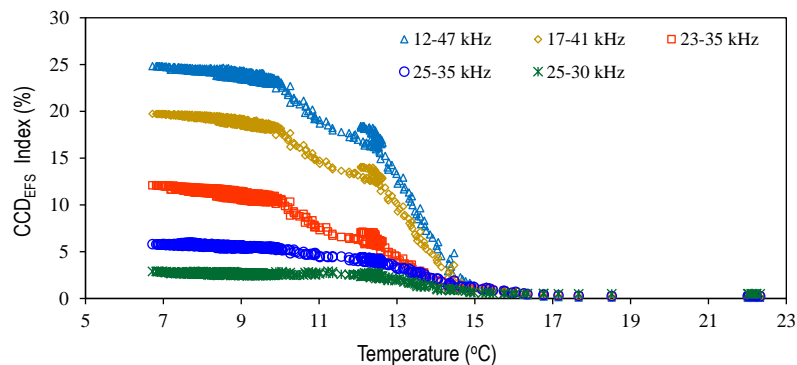


Fig. 16 CCD_{EFS} index of intact state for various frequency ranges of impedance signatures at temperatures: 6.72°C ~ 22.33°C (Reference: Test #1)

Fig. 14 shows the 1th (Test 1) and the 363th (Test 363) impedance signatures for the same frequency range (i.e., 12-47 kHz) measured at 22.33°C and 6.72°C, respectively. Note that the temperature change was approximately 16°C which was the highest temperature variation in this study. As shown in the figure, the CCD value of the two impedance patterns was significant as 59.6% due to the 16 °C temperature change. After temperature compensation using Test 1 as the reference, the CCD value was reduced to half as 24.8%, which was extremely considerable to be used as the baseline state. Fig. 15 examined two close temperatures of two consecutive days: 6.72 °C (Test 363) and 7.19 °C (Test 501). As observed from the figure, the CCD value remained the same as very small as 0.3% for before and after the EFS-based temperature compensation.

In order to select an appropriate frequency range for the temperature effect compensation, several resonant ranges of the impedance signatures (for the intact case) within 10-55 kHz were examined. Fig. 16 shows the CCD values after EFS for five tested frequency ranges: 12-47 kHz, 17-41 kHz, 23-35 kHz, 25-35 kHz, and 25-30 kHz. Note that the 1st impedance measurement at 22.33°C (Test 1) was selected as the reference impedance for the calculation. As shown in the figure, the CCD_{EFS} values obviously decreased as the temperature increased to 22.33°C for the examined frequency bands. In other word, the correlation level between two impedance signatures increased when the temperature variation decreased. It is also observed that the wider frequency bands resulted in significant CCD_{EFS} values. This demonstrates the frequency band selected for the temperature compensation should be sufficiently narrow to void false diagnoses, as discussed previously. From the analysis, the frequency range of 25-30 kHz can be selected for the temperature-effect compensation. It is worth noting that the selected frequency range may not be generalized to other target structures. The reason is that the less (or more) variation of the frequency range is dependent on the changes in the stress field of the target structure under the temperature change.

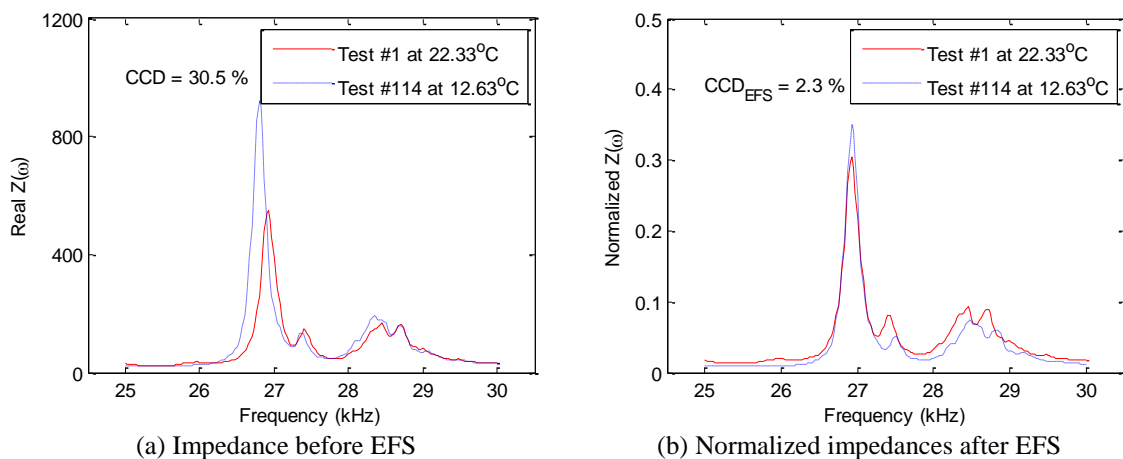


Fig. 17 Impedance signatures for frequency range 25-30 kHz measured from intact tendon-anchorage for two different temperatures: 22.3°C versus 12.63°C (Reference: Test #1)

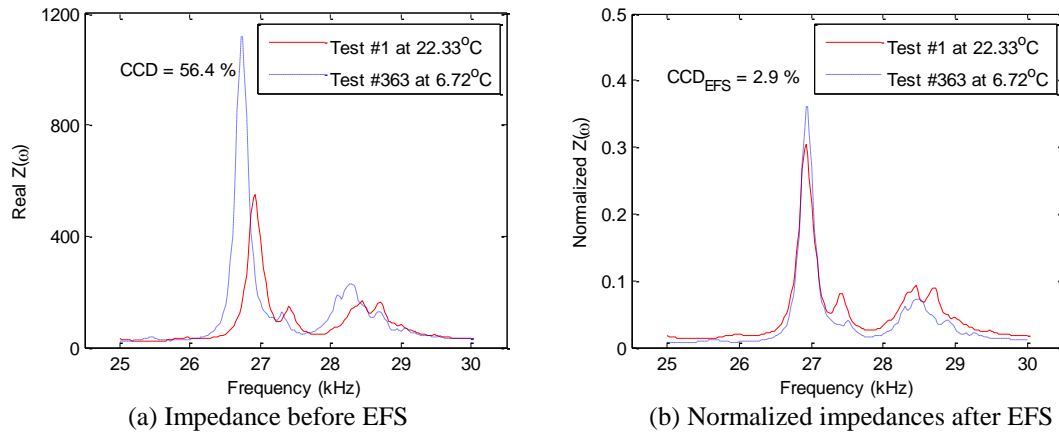


Fig. 18 Impedance signatures for frequency range 25-30 kHz measured from intact tendon-anchorage for two temperatures: 22.3°C versus 6.72°C (Reference: Test #1)

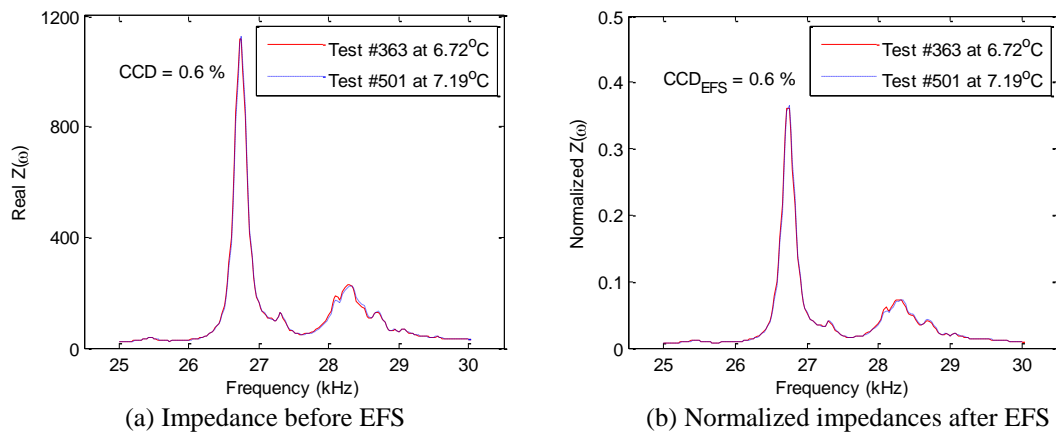


Fig. 19 Impedance signatures for frequency range 25-30 kHz measured from intact tendon-anchorage for two close temperatures: 6.72°C versus 7.16°C (Reference: Test #363)

Fig. 17 shows the 1st (Test 1) and the 114th (Test 114) impedance signatures in 25-30 kHz measured from the intact tendon-anchorage at 22.33°C and 12.63°C, respectively. Before the EFS, a considerable CCD value, 30.5%, can be observed between two impedance signatures. After the EFS, however, the CCD value was significantly reduced to 2.3%. Similarly, the CCD value between the impedance signatures of Test 1 at 22.33°C and Test 363 at 6.72°C was significantly reduced from 56.4% to 2.9% after the EFS, as observed in Fig. 18. For two consecutive days: Test 363 at 6.72°C and Test 501 at 7.19°C, the CCD value remained the same as very small as 0.6% for before and after the EFS, as shown in Fig. 19. Excellent correlations between two impedance signatures were observed over the frequency band 25-30 kHz since the resonant peaks in this band exhibited mostly the same frequency shift, as explained previously.

6.3 Prestress-loss monitoring results under temperature variation

Next, the CCD_{EFS} values were calculated for the 694 impedance measurements including 669 signals for the intact conditions (temperatures: $6.72^{\circ}\text{C} \sim 22.33^{\circ}\text{C}$) and 25 signals for five prestress levels (temperatures: $18.8^{\circ}\text{C} \sim 19.96^{\circ}\text{C}$). The impedance signals of the intact states were used to establish the upper control limit (UCL) for decision-making. For the EFS-based temperature compensation technique, the impedance signature measured at approximately the mean of the temperature variation is should be selected as the baseline impedance (Koo *et al.* 2009). Hence, the impedance measurement at 12.63°C (Test 114) was set as the reference impedance for the temperature-effect compensation.

The CCD_{EFS} indices (after temperature compensation) were computed over the wide frequency range of 12-47 kHz and the selected frequency range of 25-30 kHz, as shown in Fig. 20. When the frequency range of 12-47 kHz was employed, the UCL of the CCD_{EFS} was significant as 17.95%, as shown in Fig. 20(a). It is observed from the figure that the mountable PZT interface was failed to detect all prestress-loss levels (PS2~PS5) in the PSC girder. When the frequency range of 25-30 kHz was used, however, all prestress-loss events were successfully alarmed, as shown in Fig. 20(b). The UCL of the CCD_{EFS} index was significantly decreased to 2.1% and the CCD_{EFS} values jumped over the upper control limit even for the small prestress-loss level of 7.1% (PS2).

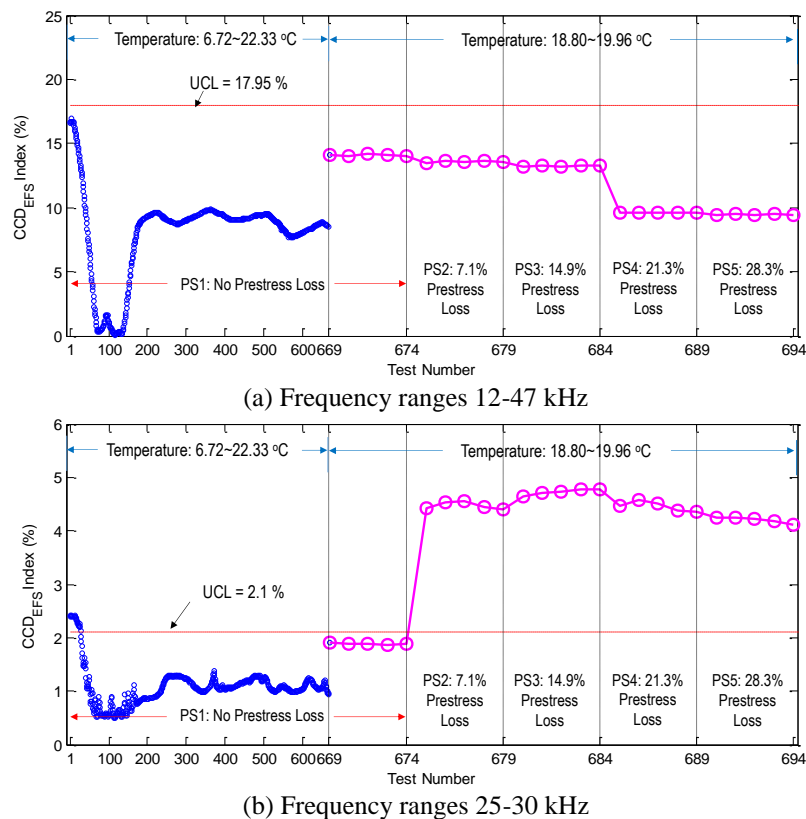


Fig. 20 Prestress-loss monitoring results under temperature variation using CCD_{EFS} index of impedance signatures (Reference: Test #114 at 12.63°C)

Basically, the damage index supposes to rise as the damage severity increases. However, as observed in Fig. 20(b), the CCD_{EFS} index increased rapidly after the first prestress-loss event, but remained mostly constant for the others. This phenomenon could be explained by the fact that the resonant peaks in 25~30 kHz exhibited mostly similar frequency shifts when the prestress-loss severity increased from PS2 to PS5 (see Fig. 12). As shown in Fig. 3(a), the similar frequency shifts of the resonant peaks will lead to unchanged values of the CCD_{EFS} index. As the result, the EFS-based technique could not recognize the change of the impedance pattern (after temperature compensation) when the prestress force reduced from PS2 to PS5. The improvement of the presented temperature compensation technique remains for the future study. Despite the above issue, these monitoring results proved the feasibility of the mountable PZT interface for alarming the prestress-loss in PSC girders under varying temperature. It is found that the CCD_{EFS} approach detected prestress-loss occurrence without knowing the temperature data of monitored states, which results in the simpler computation and the convenient data acquisition of the impedance monitoring.

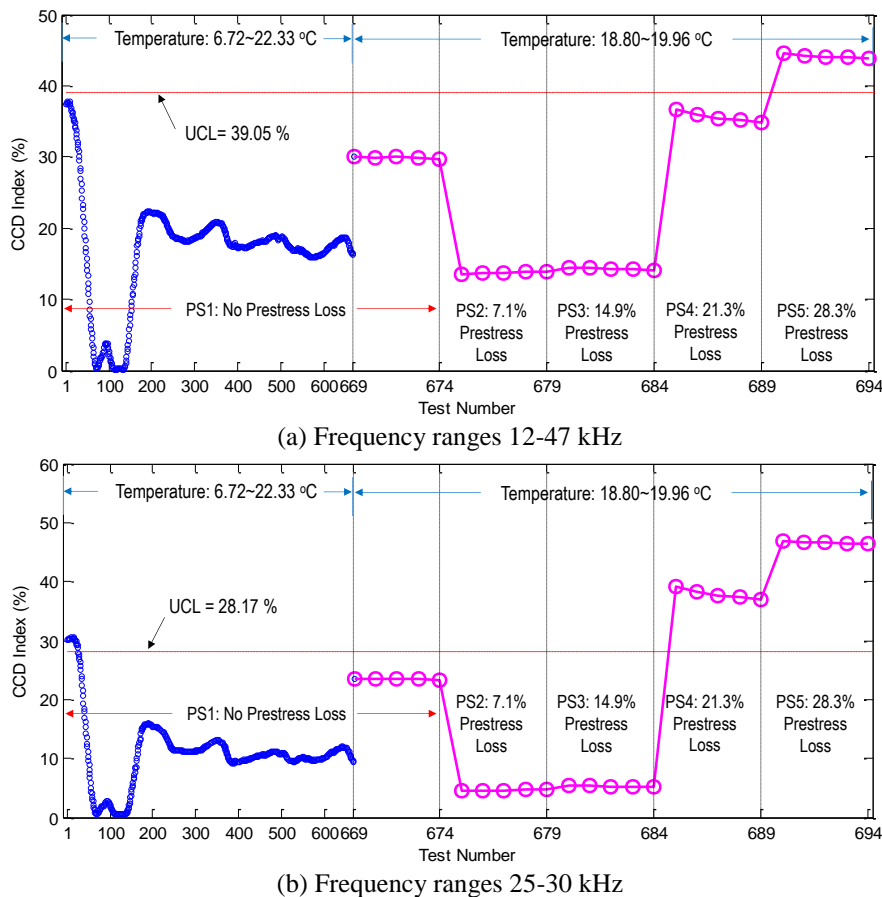


Fig. 21 Prestress-loss monitoring results under temperature variation using conventional CCD index of impedance signatures (Reference: Test #114 at 12.63°C)

For the comparison, the performance of the conventional CCD index (without temperature compensation) was examined under various temperature conditions, as shown in Fig. 21. The CCD indices were also computed for the wide frequency band of 12-47 kHz and the narrow band of 25-30 kHz. Where the wide frequency range (12-47 kHz) was employed, only the highest prestress-loss event (PS5) was successfully alarmed by the mountable PZT interface, see Fig. 21(a). A better alarming result can be found in Fig. 21(b) when using the narrow frequency band (25-30 kHz) for prestress-loss monitoring. It is observed that the mountable interface-based technique could detect the prestress losses larger than about 20 kN, but it falsely alarmed the incipient prestress-loss states (PS1~PS3) which are extremely important for structural health assessment in practice.

7. Conclusions

The prestress force in PSC girders was monitored via mountable PZT interface under varying temperature. An impedance-based technique using mountable PZT interface was proposed for prestress-loss monitoring in the tendon-anchorage. A cross-correlation-based temperature-effect compensation algorithm using the EFS of impedance signatures was outlined. Lab-scale experiments were performed on a PSC girder instrumented with a mountable PZT interface at tendon-anchorage. A series of temperature variation and prestress-loss events were simulated for the lab-scale PSC girder. The feasibility of the mountable PZT interface for prestress-loss monitoring in PSC girders was experimentally verified under constant temperature and temperature-varying conditions.

From the analyses of prestress-loss monitoring in the PSC girder, the following conclusions have been made. Firstly, the prestress-loss events in the PSC girder under unchanged temperature conditions were successfully detected by implementing the mountable PZT interface at the tendon-anchorage. The contribution of the structural impedance to the electro-mechanical impedance was considerable over the frequency range 10-55 kHz. Secondly, the mountable PZT interface successfully alarmed the prestress-loss events in the PSC girder under temperature variation by compensating the temperature effect. Thirdly, for the temperature effect compensation using the EFS-based technique, the frequency bands in which the resonant peaks exhibit mostly the same frequency shifts, should be selected. Finally, the CCD_{EFS} approach detected the prestress-loss occurrence without knowing the temperature data of monitored states; hence, it could provide the simpler computation and the convenient data acquisition for the impedance monitoring.

Acknowledgments

This work was supported by Basic Science Research Program through the National Research Foundation of Korea (NRF) funded by the Ministry of Education, Science and Technology (NRF-2013R1A1A2A10012040). The graduate student involved in this research was also supported by the Brain Korea 21 Plus program of Korean Government.

References

- Fabricio, G.B., Danilo, E.B., Vinicius, A.D.A. and Jose, A.C.U. (2014), "An experimental study on the effect of temperature on piezoelectric sensors for impedance-based structural health monitoring", *Sensors*, **14**, 1208-1227.
- Fasel, T.R., Sohn, H., Park, G. and Farrar, C.R. (2005), "Active sensing using impedance-based ARX models and extreme value statistics for damage detection", *Earthq. Eng. Struct. D.*, **34**(7), 763-785.
- Ho, D.D., Lee, P.Y., Nguyen, K.D., Hong, D.S., Lee, S.Y., Kim, J.T., Shin, S.W., Yun, C.B. and Shinozuka, M. (2012), "Solar-powered multi-scale sensor node on imote2 platform for hybrid SHM in cable-stayed bridge", *Smart Struct. Syst.*, **9**(2), 145-164.
- Hong, D.S. (2011), *Vibration-impedance-based hybrid structural health monitoring and temperature effect assessment in girder's structures*, PhD Thesis, Department of Ocean Engineering, Pukyong National University, Korea.
- Huynh, T.C. and Kim, J.T. (2014), "Impedance-based cable force monitoring in tendon-anchorage using portable PZT-interface technique", *Math. Probl. Eng.*, Article ID 784731, 1-11.
- Huynh, T.C., Park, Y.H., Park, J.H. and Kim, J.T. (2015a), "Feasibility verification of mountable PZT-interface for impedance monitoring in tendon-anchorage", *J. Shock Vib.*, **2015**, 1-11.
- Huynh, T.C., Lee, K.S. and Kim, J.T. (2015b), "Local dynamic characteristics of PZT impedance interface on tendon anchorage under prestress force variation", *Smart Struct. Syst.*, **15**(2), 375-393.
- Huynh, T.C., Park, Y.H., Park, J.H., Hong, D.S., and Kim, J.T. (2015c), "Effect of temperature variation on vibration monitoring of prestressed concrete structures", *J. Shock Vib.*, **2015**, 1-9.
- Huynh, T.C., Park, J.H. and Kim, J.T. (2016), "Structural identification of cable-stayed bridge under back-to-back typhoons by wireless vibration monitoring", *Measurement*, 10.1016/j.measurement.2016.03.032.
- Huynh, T.C. and Kim, J.T. (2016), "FOS-based prestress force monitoring and temperature effect estimation in unbonded tendons of PSC girders", *J. Aerospace Eng.*, 10.1061/(ASCE)AS.1943-5525.0000608, B4016005.
- Ko, J.M. and Ni, Y.Q. (2005), "Technology developments in structural health monitoring of large-scale bridges", *Eng. Struct.*, **27**, 1715-1725.
- Koo, K.Y., Park, S.H., Lee, J.J. and Yun, C.B. (2009), "Automated impedance-based structural health monitoring incorporating effective frequency shift for compensating temperature effects", *J. Intel. Mat. Syst. Str.*, **20**, 367-377.
- Kim, J.T., Huynh, T.C. and Lee, S.Y. (2014), "Wireless structural health monitoring of stay cables under two consecutive typhoons", *Struct. Monit. Maint.*, **1**(1), 47-67.
- Kim, J.T., Nguyen, K.D. and Huynh, T.C. (2013), "Wireless health monitoring of stay cable using piezoelectric strain response and smart skin technique", *Smart Struct. Syst.*, **12**(3-4), 381-379.
- Kim, J.T., Na, W.B., Park, J.H. and Hong, D.S. (2006), "Hybrid health monitoring of structural joints using modal parameters and EMI signatures", *Proceeding of SPIE*, San Diego, USA.
- Kim, J.T., Park, J.H., Hong, D.S. and Park, W.S. (2010), "Hybrid health monitoring of prestressed concrete girder bridges by sequential vibration-impedance approaches", *Eng. Struct.*, **32**, 115-128.
- Kim, J.T., Yun, C.B. and Yi, J.H. (2003), "Temperature effects on frequency-based damage detection in plate-girder bridges", *J. KSCE*, **7**(6), 725-733.
- Li, H.N., Yi, T.H., Ren L., Li, D.S. and Huo, L.S. (2014), "Review on innovations and applications in structural health monitoring for infrastructures", *Struct. Monit. Maint.*, **1**(1), 1-45.
- Liang, C., Sun, F.P. and Rogers, C.A. (1994), "Coupled electro-mechanical analysis of adaptive material - Determination of the actuator power consumption and system energy transfer", *J. Intel. Mat. Syst. Str.*, **5**, 12-20.
- Lynch, J.P., Wang, W., Loh, K.J., Yi, J.H. and Yun, C.B. (2006), "Performance monitoring of the Geumdang Bridge using a dense network of high-resolution wireless sensors", *Smart Mater. Struct.*, **15**(6), 1561-1575.

- Mascarenas, D.L., Todd, M.D., Park, G. and Farrar, C.R. (2007), "Development of an impedance-based wireless sensor node for structural health monitoring", *Smart Mater. Struct.*, **16**(6), 2137-2145.
- Min, J.Y. (2012), *Structural health monitoring for civil infrastructure using wireless impedance sensor nodes and smart assessment techniques*, PhD Thesis, Department of Civil and Environmental Engineering, KAIST, Korea.
- Nguyen, K.D. and Kim, J.T. (2012), "Smart PZT-interface for wireless impedance-based prestress-loss monitoring in tendon-anchorage connection", *Smart Struct. Syst.*, **9**(6), 489-504.
- Park, J.H., Kim, J.T., Hong, D.S., Mascarenas, D. and Lynch, J.P. (2010), "Autonomous smart sensor nodes for global and local damage detection of prestressed concrete bridges based on accelerations and impedance measurements", *Smart Struct. Syst.*, **6**(5-6), 711-730.
- Park, J.H., Huynh, T.C. and Kim, J.T. (2015), "Temperature effect on wireless impedance monitoring in tendon anchorage of prestressed concrete girder", *Smart Struct. Syst.*, **15**(4), 1159-1175.
- Park, G., Kabeya, K., Cudney, H. and Inman, D. (1999), "Impedance-based structural health monitoring for temperature varying applications", *JSME Int. J. Ser. A Solid Mech. Mater. Eng.*, **42**, 249-258.
- Rice, J.A., Mechtov, K., Sim, S.H., Nagayama, T., Jang, S., Kim, R., Spencer, Jr, B.F., Agha, G. and Fujino, Y. (2010), "Flexible smart sensor framework for autonomous structural health monitoring", *Smart Struct. Syst.*, **6**(5-6), 423-438.
- Sepehry, N., Shamshirsaz, M. and Abdollahi, F. (2011), "Temperature variation effect compensation in impedance-based structural health monitoring using neural networks", *J. Intel. Mat. Syst. Str.*, **20**(10), 1-8.
- Siebel, T. and Lilov, M. (2013), "Experimental investigation on improving electromechanical impedance based damage detection by temperature compensation", *Key Eng. Mater.*, **569-570**, 1132-1139.
- Sohn, H. (2007), "Effects of environmental and operational variability on structural health monitoring", *Philos. T. R. Soc. A*, **365**, 539-560.
- Sun, F.P., Chaudhry Z., Liang, C. and Rogers C.A. (1995), "Truss structure integrity identification using PZT sensor-actuator", *J. Intel. Mat. Syst. Str.*, **6**, 134-139.
- Yun, C., Cho, S., Park, H., Min, J. and Park, J. (2013), "Smart wireless sensing and assessment for civil infrastructure", *Struct. Infrastruct. Eng. Maint. Manag. Life-Cycle Design Perform.*, **10**(4), 534-550.
- Zagrai, A.N. and Giurgiutiu, V. (2001), "Electro-mechanical impedance method for crack detection in thin plates", *J. Intel. Mat. Syst. Str.*, **12**, 709-718.